J Mater Sci: Mater Electron (2023)34:1735

Architecture of γ-WO_3 nanosheets-like electrode material for super capacitor application

Rahul S. Diggikar[1,*], Mohaseen S. Tamboli[2], S. K. Shinde[3], Shamkumar P. Deshmukh[4], Shoyebmohamad F. Shaikh[5], Hassnain Abbas Khan[6], and Nguyen Tam Nguyen Truong[7,*]

[1] *Department of Chemistry, New Arts, Commerce and Science College, Parner, Ahmednagar, Maharashtra 414302, India*
[2] *Korea Institute of Energy Technology (KENTECH), 21 KENTECH-gil, Naju, Jeollanam-Do 58330, Republic of Korea*
[3] *Department of Physics, Arts, Science and Commerce College, Indapur, Maharashtra 413106, India*
[4] *Department of Chemistry, D.B.F. Dayanand College of Arts and Science, Solapur, MS 413002, India*
[5] *Department of Chemistry, College of Science, King Saud University, P.O. Box 2455, 11451 Riyadh, Saudi Arabia*
[6] *Clean Energy Research Centre, Korea Institute of Science and Technology, Cheongryang, PO Box 131, Seoul 02-792, Republic of Korea*
[7] *School of Chemical Engineering, Yeungnam University, 280 Daehak-Ro, Gyeongsan 38541, Republic of Korea*

Received: 3 April 2023
Accepted: 28 July 2023

ABSTRACT

The present work demonstrated simple, cost-effective, and efficient synthetic approach for producing two-dimensional (2D) nanosheets (NSs) of oxygen-deficient monoclinic γ-tungsten oxide (γ-WO_3), which exhibit desirable properties used for super capacitor application. The hydrothermal method was employed at a temperature of 120 °C for 12 h to synthesize γ-WO_3. Structural and optical properties of the γ-WO_3 NSs were analyzed by using various techniques such as X-ray diffraction, Raman spectroscopy, diffused reflectance spectroscopy, and photoluminescence analysis. Morphological characterization was performed using field emission-scanning electron microscopy and high-resolution transmission electron microscopy. Furthermore, the electrochemical properties of the γ-WO_3 NSs were evaluated for supercapacitor applications. The as-synthesized γ-WO_3 NSs electrode exhibited a remarkable specific capacitance of 386 F g^{-1} at a low current density of 5 mA cm^{-2}. Also, the γ-WO_3 NSs electrode displayed excellent stability, emphasizing its potential for energy storage device applications (ESDA).

Address correspondence to E-mail: diggikarrs@gmail.com; tamnguyentn@ynu.ac.kr

https://doi.org/10.1007/s10854-023-11081-7
Published online: 30 August 2023

1 Introduction

Nanomaterial with two-dimensional (2D) structures have received immense attention owing to their specific structural anisotropy and several fascinating electrical properties [1–3]. The transition metal oxide (TMO) semiconductors [4–11] with well-known physical and chemical properties in hierarchical nanostructures have attentive for wide applications in electrochemical energy storage devices (EESDs). However, the electrochemical activity of nanostructure tungsten oxides (WO_3) strongly depends on morphology and crystal system based on synthesis techniques, besides this, are also useful in water splitting, [12] visible light driven photo catalysts, photochromic devices, buffer layer in organic light-emitting diodes and sensor. EESDs play the central role in ongoing sustainable carbon-free energy technologies such as solar cells, batteries, and super capacitors, where the key factor in up and down streams of energy and power density devices trying to be resolved for both the purpose of TMOs are preferred. Due to the excellent electrochemical stability, low cost and easy to obtained WO_3 motivated to the material scientist to make a new avenue in the field of EESDs [13]. The recognition of these technologies heavily trusts on the fundamental properties of the electrode materials that are being used to fabricate EESDs. WO_3 has been materialized as a projecting metal oxide for next EESDs development by its inherently tunable nonstoichiometric, surface-active redox states augmented to improve the electrode kinetics in super capacitor applications. For the same, various synthesis techniques have been employed to engineer 2D materials with designated and controllable morphology. [14, 15] Recently, Mandal et al. [16] reported the lack of synthesis techniques with high quality WO_3 nanostructures. Yin et al. [17] presented the NSs of anchored WO_3. The quality of nanostructures used for the supercapcitor is depends on the contact between electrode and electrolyte, the NSs possesses the sufficient area for the contact due to aspect ratio. Yang et al. [18] reported the NSs of WO_3 doped with $MnO_{2\ for}$ super capacitor. The quality of nanophase WO_3 also been improved by compositing with post transition metals [19].

In the context, the 2D γ WO_3 Nano sheets (NSs) is synthesized by hydrothermal technique in mild conditions and tested for electrode material in super capacitor applications resulting as a promising material. By using the nanostructures reported the enhanced nano-technological applications. The super capacitor is one of the most important EESD which works as a faster delivery of energy than batteries and is superior to conventional capacitors [20]. To date, various electrode materials have been synthesized for use in supercapacitors, including conducting polymers, metal–organic frameworks, siloxenes, transition metal oxides, transition metal sulfides, carbonaceous materials, chalcogenides, polyoxometalates [5, 9, 11], Tungsten oxides in the forms of NSs is an n-type semiconductor with an indirect bandgap having good optical, chemical, and thermal stability, making it appropriate for super capacitor applications [21–23]. Extensive research and numerous studies have focused on WO_3 based super capacitors, highlighting their notable pseudo capacitive behavior arising from the presence of multiple oxidation states, rapid surface reactions, and a crystal structure conducive to the intercalation of electrolyte ions. Huang et al. [24] observed a high specific capacitive of WO_3 NSs.

In this work, we report the synthesis of stable, cost-effective, and oxygen deficient 2D-γ- WO_3 NSs by hydrothermal method and their performance in super capacitor applications. The synthesized materials were characterized by different spectroscopic techniques. Then, the as-synthesized materials were tested for super capacitive properties in the three-electrode system with the potential window of 0.0–0.6 V in the presence of 3 M KOH. The as-synthesized 2D NSs of γ- WO_3 demonstrated excellent electrochemical performance with the specific capacitance of 386 F g^{-1} at a constant current density of 5 mA cm^{-2}.

2 Experimental section

2.1 Synthesis of γ-Tungsten oxide nanosheet (γ-WO_3 NSs)

The precursors used in this synthesis are of analytical grade and utilized as received. In a typical reaction, an equivalent amount of lead acetate $Pb(C_2H_3O_2)_2$ and sodium tungstate (Na_2WO_4) (2 mmol) were dissolved in 50 ml 0.1 M nitric acid (HNO_3) solution. The mixture was stirred vigorously for 75 min in a hot water bath and obtained a white color suspension. This white color suspension of lead tungstate

($PbWO_4$) turns to yellow at pH 2.9 [15] which is subjected to the hydrothermal treatment at 120 °C for 12 h in a Teflon reactor jacketed with stainless steel autoclave. After the completion of the reaction, the product was filtered at room temperature and then washed with DI water and dried at 100 °C for 2 h.

2.2 Characterizations

The structural analysis and phase purity of the sample was examined by X-ray diffraction (XRD) on a Bruker D8 Advance X-ray diffractometer. X-ray photoelectron spectroscopy (XPS) analysis was performed using an ESCALAB-MKII spectrometer. The absorption properties were measured by a UV–Vis diffuse reflectance spectrophotometer (UV-3600, Shimadzu). The Photoluminescence properties were measured by a spectrofluorophotometer (RF-5301PC, Shimadzu). Room-temperature micro-Raman scattering analysis was performed using an HR 800-Raman spectrometer (Horiba Jobin Yvon), with excitation at 532 nm. The morphological features of the synthesized samples were analyzed by Field-Emission Scanning Electron Microscopy (HITACHI S4800) and Transmission Electron Microscopy (FEI Technai T20, Netherlands). For SEM analysis, the sample was mounted on an aluminum stub using conductive sticky pads. For TEM analysis, the as-synthesized sample was dispersed onto TEM grids using ethanol, and air-dried before imaging.

2.3 Electrochemical measurement

Electrochemical properties of the electrodes fabricated from nanosheet-like γ-WO_3 were measured through a three-electrode assembly in 3 M KOH electrolyte using a Versa STAT 3 electrochemical workstation. The three-electrode assembly was composed of WO_3 as a working electrode, platinum as a counter electrode, and saturated calomel electrode (SCE) as a reference electrode. The cyclic voltammetry (CV) analysis was performed by varying the scan rates from 5 to 100 mV s^{-1} within a potential window of 0–0.6 V vs. SCE. A Galvanostatic charge–discharge (GCD) investigation was carried out at various current densities ranging from 5 to 10 mA cm^{-2}. The electrochemical impedance spectroscopy (EIS) was conducted over a frequency range of 1 Hz–100 kHz.

3 Results and discussion

Figure 1a–d illustrates the XRD, Raman, DRS, and PL study of γ-WO_{3-x} NSs, respectively. The peak positions in Fig. 1a correspond to the monoclinic structure of WO_3 (γ-WO_3) with lattice parameters, a = 0.7301, b = 0.7539, and c = 0.7688 nm (JCPDS Card No 01-083-0950). The monoclinic structure of WO_3 is referred to as the gamma phase of tungsten oxide (γ-WO_3). The strong intensity peak located at 23.1° indicates domination of the (002) crystal plane as a preferred orientation [25]. Comparison to the XRD pattern of bulk WO_3 reported by Boruah et al., [26] corresponds to γ-WO_3 NSs. In addition, the shape of the peak located at 34.19° is not the same as bulk WO_3. This could indicate the oxygen deficiency in WO_3 NSs [15]. The Raman peaks observed at 720 and 813.5 cm^{-1} in Fig. 1b correspond to the stretching vibrations [υ (O-W-O)] and the peak at 280.5 cm^{-1} belongs to the bending vibrations [δ (O-W-O)] of the γ-WO_3 NSs [27–29]. Unlike in the bulk WO_3, the peaks are slightly blue-shifted, this again could attribute to the oxygen deficiency in the NS [23]. From the UV–Vis diffuse reflectance spectrum shown in Fig. 1c., the electronic band gap of the NSs is estimated as 2.86 eV. The band gap was evaluated by the Tauc method using the following Eq. (1):

$$(\alpha.h\nu)^{1/\gamma} = B(h\nu - E_g) \quad (1)$$

where, α is the absorption coefficient, h is the Planck constant, ν is the photon's frequency, E_g is the band gap energy and B is a constant. The γ factor depends on the nature of the electron transition and is equal to 1/2 for direct and 2 for indirect band gaps. [26] The band gap of the NSs is higher than that of the commercial bulk WO_3 (2.54 eV) partially due to quantum confinement effects [15]. The major cause of the enhancement in the band gap is due to the shortage of O^{2-} ions at the intrinsic sites, although oxygen deficiency ultimately helps in the formation of the NSs [26, 27]. Fig. 1d reveals the PL spectrum of γ-WO_3 NSs obtained at an excitation wavelength of 325 nm in dichloromethane. The strong peak at 433 nm reveals a bandgap of 2.86 eV (∼ transparent WO_3) and other weak peaks are at the border of quantum confinement. However, quantum confinement is difficult to attain in metal oxides because their exciton Bohr radii are of the order of a nanometer [28]. This border quantum confinement

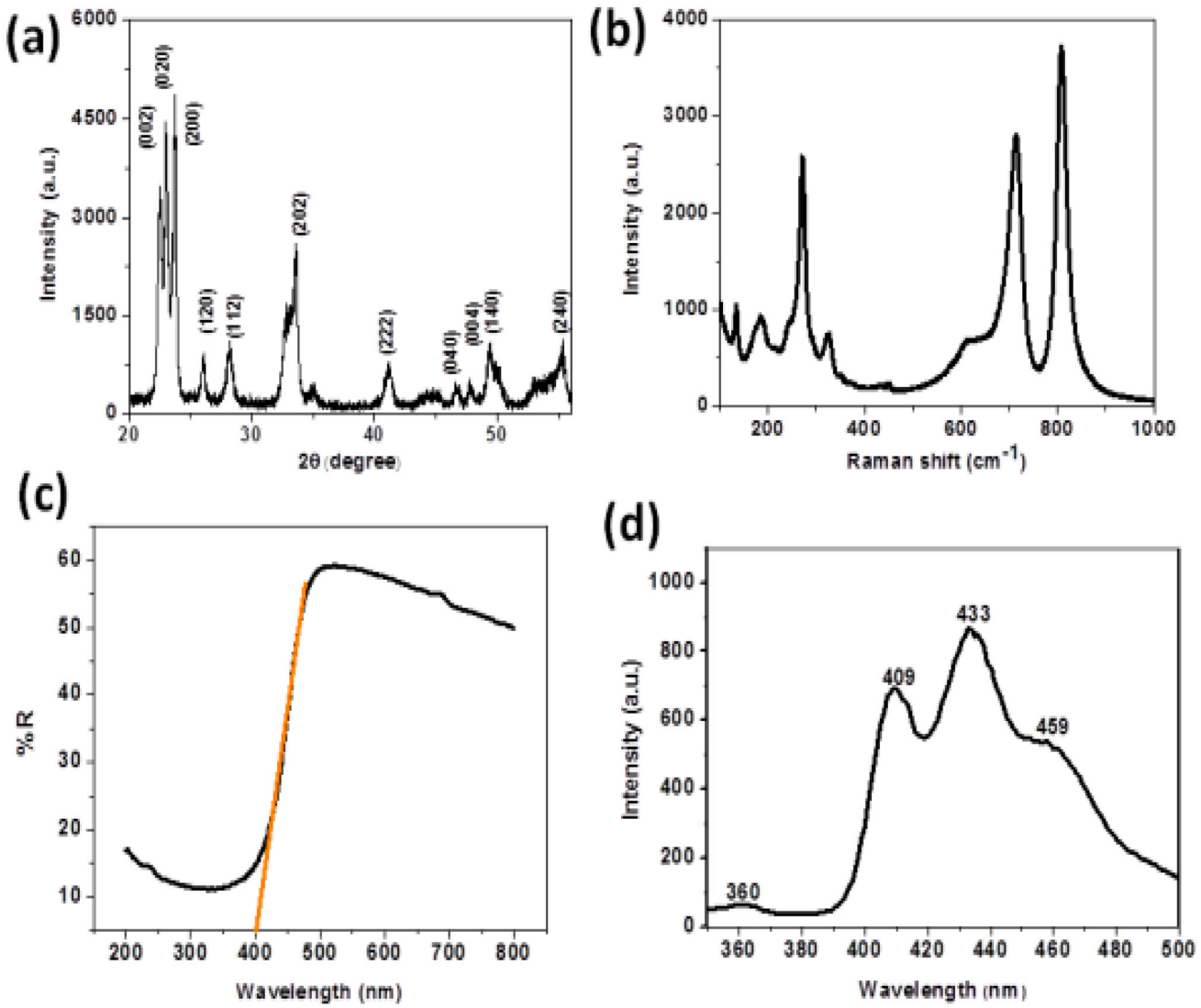

Fig. 1 **a** XRD, **b** Raman spectra, **c** Diffused reflectance spectra (DRS), and **d** Photoluminescence (PL) of γ-WO_3 NSs

and oxygen deficiency are indicated by the peaks at 433 and 459 nm, respectively.

The possible reaction of our as-prepared samples is given as follows. The reactions involved as,

$$PbAC_2 + Na_2WO_4 \xrightarrow{\Delta} PbWO_4 + 2NaAC$$

$$PbWO_4 + 2H^+ \rightarrow PbWO_3H_2O \rightarrow WO_3 + H_2O$$

FE-SEM images of the γ-WO_3 NSs with different magnifications are displayed in Fig. 2a and b. From Fig. 2a, the morphology of the as-synthesized γ-WO_3 can be concluded as NSs. From the high magnification image provided in Fig. 2b, the average lateral size and thickness of the NSs are estimated to be 50 and 100 nm respectively. It shows that these NSs are loosely stacked together leading to a large mesoporosity, which could be one of the factors contributing to the good electrochemical properties. The surface area plays an important role in enhancing the supercapacitor properties. Therefore, the 2D NSs can provide better optimization routes including the modulation of the materials' activity, surface polarization, and rich oxygen vacancies. Hence, this is synthesized γ-WO_3 NSs could be very effective for supercapacitor applications.

The TEM images of γ-WO_3 NSs are given in Fig. 2c and d show the growth of a thin layer of uniform γ-WO_3 NSs. Figure 2c show γ-WO_3 NSs with irregular morphology. By analyzing the TEM images (Fig. 2c),

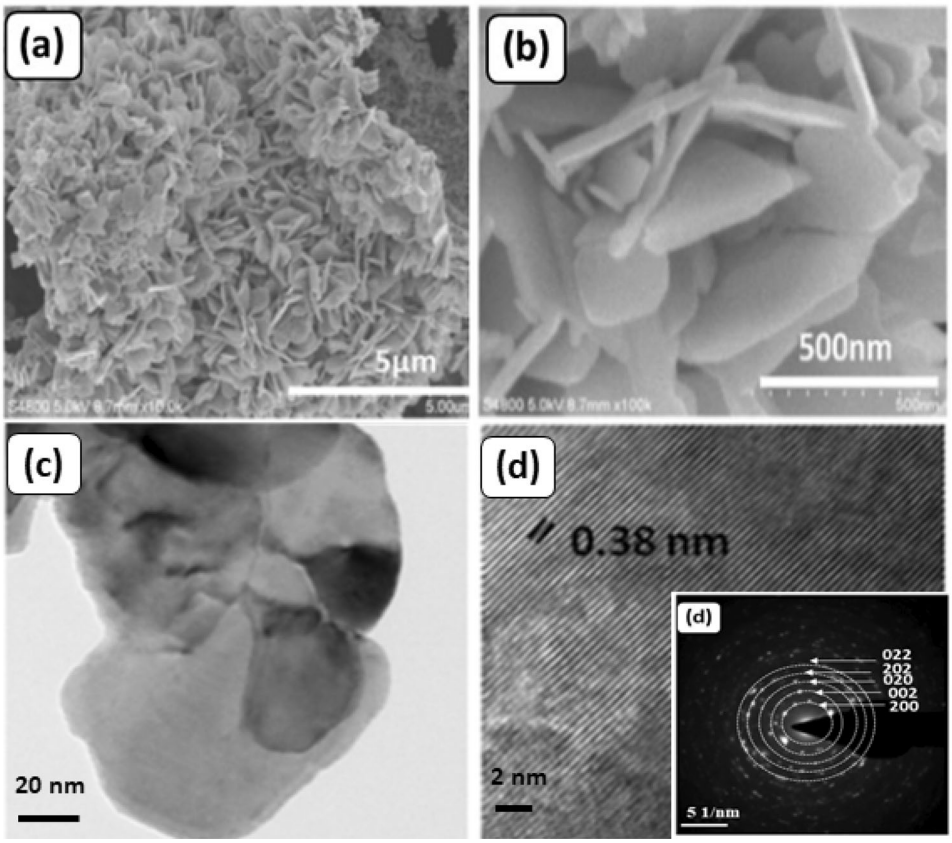

Fig. 2 **a**–**b** FESEM images of γ-WO_3 NSs **c** TEM images of γ-WO_3 NSs **d** high resolution image and SAED pattern (inset) of γ-WO_3 NSs synthesized by hydrothermal method

it is estimated that γ-WO_3 NSs have a broad distribution in lateral size ranging from 20 to 100 nm. The observed NSs-like morphology is favorable for supercapacitor application. HR-TEM images of the NSs displayed in Fig. 2d, clearly show lattice fringes, whose resolution is estimated to be 0.38 nm. This corresponds to the interplanar distance of the (002) planes of WO_3 (in good agreement with JCPDS data 01-083-0950), supporting the dominance of (002) peaks in the XRD patterns shown in Fig. 2a. The SAED pattern of the NS is given in inset Fig. 2d. From the figure, it is clear that the NS are crystalline and the corresponding planes match very well with the XRD data given in (Fig. 1a).

Elemental and oxidation state analysis was performed using XPS and are presented in Fig. 3a–c. The XPS survey spectrum of the NSs presented in Fig. 3a displays no other peaks than that of 'W' and 'O'. The W4f spectrum with spin–orbit doublet 7/2–5/2 for the 'W' valance state is demonstrated in Fig. 3b. In Fig. 3c, the deconvoluted O1s spectra of the γ-WO_3 NSs are displayed. The peak located at 529.6 and 530 eV corresponds to the stoichiometric O_2^- ions, while the slightly shifted peak located at 532.5 eV corresponds to oxygen deficiency [15]. The XPS results further support the XRD and Raman data to confirm the presence of oxygen deficiency in the nanosheet [29].

Figure 4 shows the supercapacitive properties of the γ-WO_3 thin films prepared using the hydrothermal method at a temperature of 120 °C for a constant deposition time of 12 h. Figure 4a shows the CV measurements of the γ-WO_3 thin films with various scan rates from 5 to 100 mV s^{-1} in the potential window of 0 to − 0.6 V, respectively. The CV curves indicate the scan rates increase in the area under the CV curves and the reduction peaks intensity also increases. The values of specific capacitances of the γ-WO_3 thin film can be calculated using standard relations [29]. The calculated values of the Cs are shown in Fig. 4b, the obtained Cs values of 451, 409, 314, 190, 171, and 161 F g^{-1} for 5, 10, 20, 50, 80, and 100 mV s^{-1}, respectively. The Cs values of the γ-WO_3 thin film show larger than the reported values in the literature review. The calculated values of Cs are more than the previously reported values because the vertical growth of the nanoplates like surface morphology provided higher surface area and easy axis

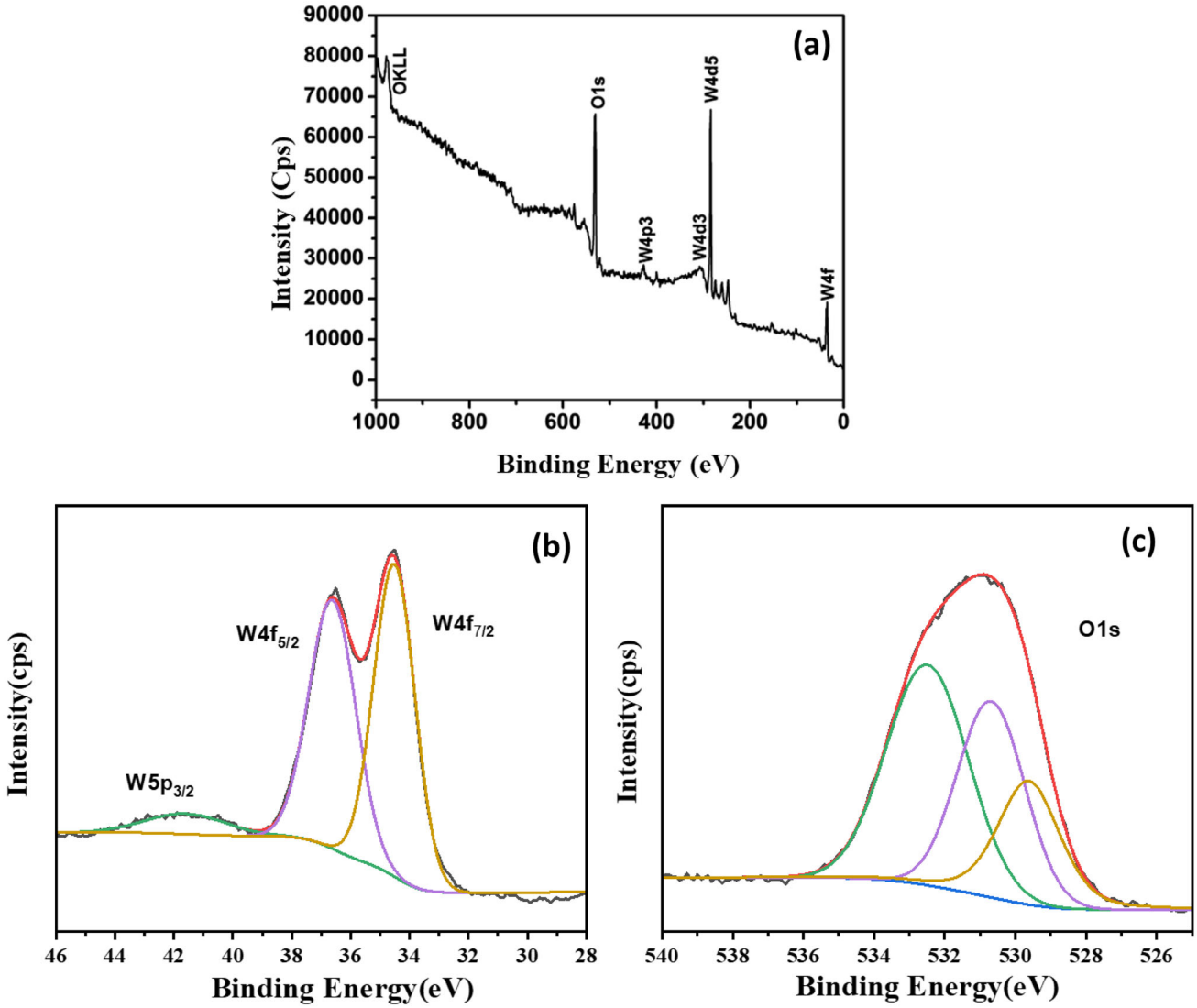

Fig. 3 **a** XPS survey scan spectrum **b** W4f XPS spectrum, and **c** O1s XPS spectrum of γ-WO_3 NSs

of the ions transfer from the electrode/electrolyte interface. Numerous researchers are currently engaged in the study of WO_3 nanomaterial for its potential use in electrochemical applications [30]. Sun et al. [31] synthesized the hexagonal nanorod-like WO_3 electrodes for negative electrode material by hydrothermal method for the supercapacitors application, and they reported a higher specific capacitance of 415.3 F g^{-1} at 0.5 A g^{-1}. Mineo et al. [32] reports the WO_3 electrode material using hydrothermal method. Also they reported the value specific capacitance of 325 F g^{-1} at fixed scan rate 2 mV s^{-1} with hexagonal nanostructures. Also, they reported the effect of, structural morphology and electrical properties of WO_3 electrodes. Similarly, the supercapacitor properties of the as-synthesized nanoplates like the nanostructure of γ-WO_3 thin films were studied by GCD measurements with the same potential window (0.0 to − 0.6 V) in the 3 M KOH electrolyte. Figure 4c shows the typical GCD measurements of γ-WO_3 thin films at different current densities from 5 to 10 mA cm^{-2} in the constant potential windows of 0.0 to 0–0.6 V, respectively. The charging-discharging curves show a non-linear-like nature which is typical behavior of electrical double layer capacitor (EDLC) super capacitors. This types of behavior indicate the presence of faradaic reaction in the as-synthesized nanoplates like γ-WO_3 thin films and electrolytes. The calculated values of the Cs of the as-synthesized nanoplates like γ-WO_3 thin films

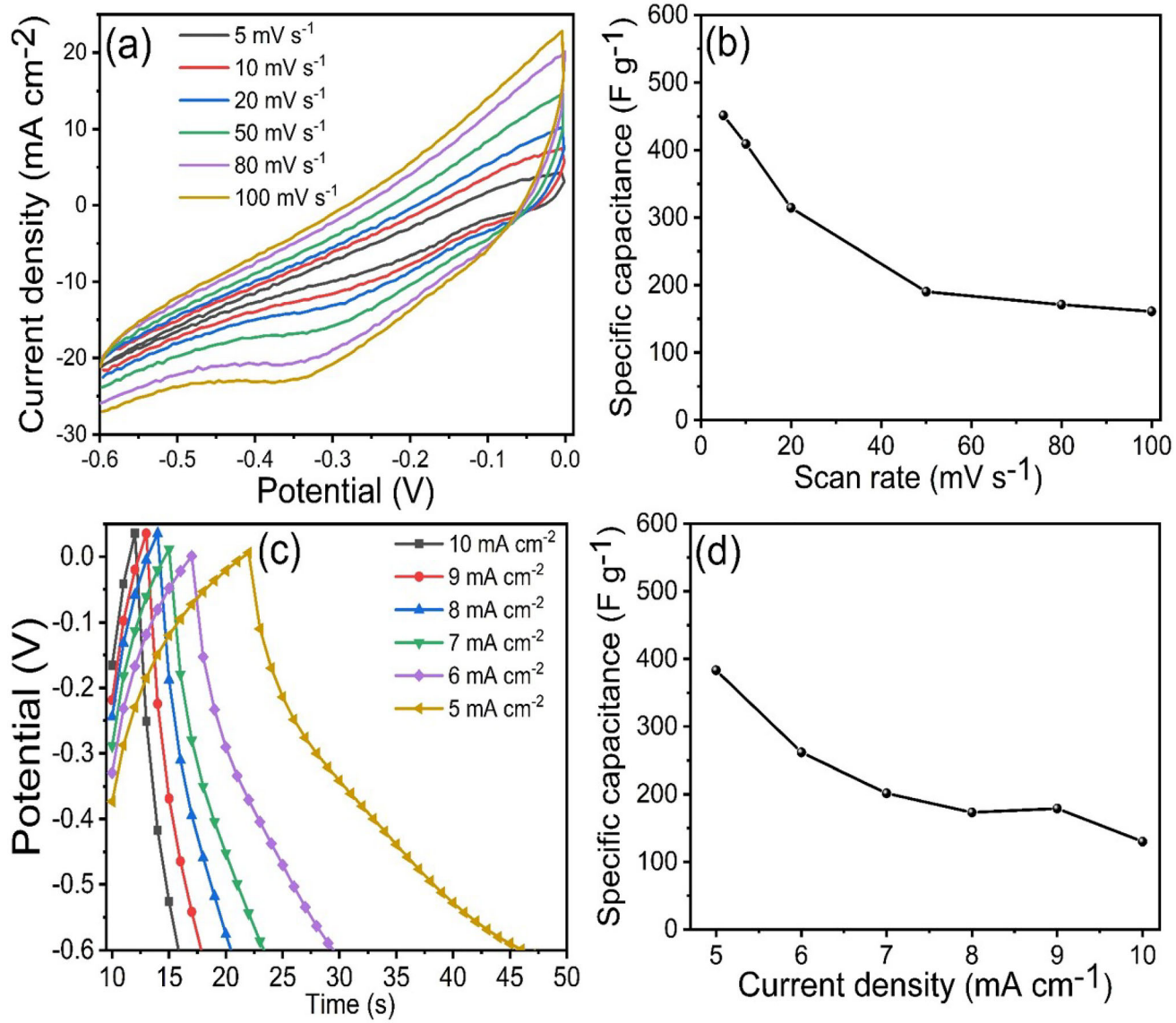

Fig. 4 **a** CV curves of WO_3 electrodes at various scan rates, **b** specific capacitance with scan rates, **c** GCD curves of WO_3 electrodes at different current densities, and **d** specific capacitance with different current density

using standard relations. The calculated Cs values were 383, 261, 201, 173, 179, and 130 F g^{-1} at different current densities of 5, 6, 7, 8, 9, and 10 mA cm^{-2} (as shown in Fig. 4d) [32–35]. Kumar and Karuppuchamy [36] prepared the Co doped WO_3 electrode composite with CNT using solution growth method. They mentioned the value of the specific capacitance of 60 F g^{-1} at 1 A g^{-1}, respectively. The calculated Cs values are better than the previously mentioned study [37], which indicates the highly porous-like surface supply more active surface area for electrochemical properties, which is useful for faster ion transformation during the electrochemical reaction [33, 34].

For more details study of the electrical mechanism of the as-synthesized nanoplates like a γ-WO_3 thin film as shown in Fig. 5. We used the EIS techniques in the constant frequency of 1–100 kHz with an open-potential 0.39 V. The calculated values of the solution resistance (R_s) and charge-transfer resistance (R_{ct}) of

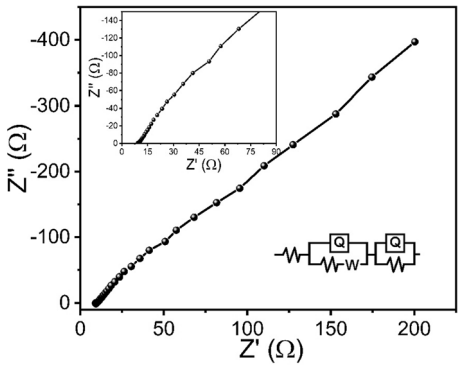

Fig. 5 EIS plots of WO_3 electrode, inset shows zoom image of the EIS and equivalent circuit

γ-WO_3 thin film fitted data with the Z-SimpWin software. The fitted data provided the values of the R_s and R_{ct} are 9.1 and 1.19 Ω, respectively. The calculated values of the charge-transfer resistance indicate the as-synthesized nanoplates like γ-WO_3 electrode provided higher conductivity for the enhanced electrochemical properties [34, 35].

4 Conclusions

In conclusion, high-quality γ-WO_3 NSs were synthesized by an inexpensive hydrothermal route at low temperatures. The as synthesized materials were characterized by different techniques such as X-ray diffraction, Raman spectroscopy, diffused reflectance spectroscopy, and photoluminescence analysis, field emission-scanning electron microscopy and high-resolution transmission electron microscopy. The as-prepared γ-WO_3 NSs have a monoclinic structure with the (002) plane as the preferred orientation. The as-synthesized γ-WO_3 has nanosheet-like morphology having a thickness of ∼ 50 nm. The band gap of the nanosheet is calculated to be 2.86 eV using DRS results. In the Raman study of γ-WO_3 NSs, the peaks at 720 and 813.5 cm^{-1} corresponds to the stretching vibrations [υ (O-W-O)] and 280.5 cm^{-1} belong to the bending vibrations [δ (O-W-O)]. Furthermore, γ-WO_3 NSs were tested for electrochemical properties for supercapacitor application. The as-synthesized γ-WO_3 NSs electrode shows a high specific capacitance of 451 F g^{-1} at a scan rate of 5 mV s^{-1}. In addition, the γ-WO_3 nanosheet electrode displayed excellent stability, emphasizing its potential for energy storage applications. It opens up a new avenue to produce a new phase of WO_3 that will be extremely useful for supercapacitor applications as well as other opto-electronic applications such as a photodetector, photo-switches, high-performance ultraviolet radiation sensors, optical keys, optical memory, etc. Further research in this direction is highly anticipated.

Author contributions

Conceptualization, writing-original draft, and methodology, RSD; formal analysis, MST, and SKS; resources. SPD; HK; writing—review and editing, SFS and NTNT funding acquisition, SFS, All authors have read and agreed to the published version of the manuscript.

Funding

The authors extend their sincere appreciation to the Researchers Supporting Project number (RSP2023R370), King Saud University, Riyadh, Saudi Arabia for the financial support.

Data availability

Not Applicable.

Declarations

Conflict of interest The authors declare that they have no conflict of interest.

Research involving human and animal participants This article does not contain any studies with human participants or animals performed by any of the authors. In this experiment, we did not collect any samples of human and animals.

References

1. S. Chen, J. Duan, Y. Tang, B. Jin, S.Z. Qiao, Molybdenum sulfide clusters-nitrogen-doped graphene hybrid hydrogel film as an efficient three-dimensional hydrogen evolution electrocatalyst. Nano Energy **11**, 11–18 (2015)
2. X. Wang, G. Li, F.M. Hassan, M. Li, K. Feng, X. Xiao, Z. Chen, Building sponge-like robust architectures of CNT–graphene–Si composites with enhanced rate and cycling

performance for lithium-ion batteries. J. Mater. Chem. A **3**, 3962–3967 (2015)
3. J. Low, S. Cao, J. Yu, S. Wageh, Two-dimensional layered composite photocatalysts. Chem. Commun. **50**, 10768–10777 (2014)
4. P. Velusamy, R. Ramesh Babu, K.T., Aparna, effect of Sm doping on the physical properties of ZnO thin films deposited by spray pyrolysis technique. AIP Conference Proceedings **1832**, 080085 (2017). https://doi.org/10.1063/1.4980545
5. R.S. Diggikar, M.V. Kulkarni, G.M. Kale, B.B. Kale, Formation of multifunctional nanocomposites with ultrathin layers of polyaniline (PANI) on silver vanadium oxide (SVO) nanospheres by in situ polymerization. J. Mater. Chem. A **1**, 3992–4001 (2013)
6. S.P. Deshmukh, K.R. Sanadi, R.S. Diggikar, V.B. Koli, A.V. Mali, Structural, magnetic, and electrical properties of manganese-substituted magnesium chromate spinel structure. J. Mater. Sci.: Mater. Electron. **32**, 6810–6819 (2021)
7. P. Velusamy, R.R. Babu, K. Ramamurthi, Structural, microstructural, optical and electrical properties of spray deposited rare-earth metal (Sm) ions doped CdO thin films. J. Mater. Sci.: Mater. Electron. **26**, 4152–4164 (2015)
8. P. Velusamy, R. Ramesh Babu, K. Ramamurthi, M.S. Dahlem, E. Elangovan, High transparent conducting cerium incorporated CdO thin films deposited by spray pyrolytic technique. RSC Adv. **0**, 1–3 (2013)
9. R.S. Diggikar, J.D. Ambekar, M.V. Kulkarni, B.B. Kale, Nanocrystalline silver vanadium sulfide (SVS) anchored polyaniline (PANI): new nanocomposite system for supercapacitor, 2013. New J. Chem. **37**(10), 3236–3243 (2013)
10. P. Velusamy, R. Ramesh Babu, K. Ramamurthi, E. Elangovan, J. Viegas, Effect of La doping on the structural, optical and electrical properties of spray pyrolytically deposited CdO thin films. J. Alloys Compd. **708**, 804–812 (2017)
11. R.S. Diggikar, V.M. Dhavale, D.B. Shinde, N.S. Kanbargi, M.V. Kulkarni, B.B. Kale, Morphology controlled synthesis of LiV 2 0 5/Ag nanocomposite nanotubes with enhanced electrochemical performance. RSC Adv. **2**, 3231–3233 (2012)
12. P. Velusamy, X. Liu, M. Sathiya, N.S. Alsaiari, F.M. Alzahrani, M. Tariq Nazir, M. Elangovan Elamurugu, Senthil Pandian, Fuchun Zhang, Investigate the suitability of g-C_3N_4 nanosheets ornamented with BiOI nanoflowers for photocatalytic dye degradation and PEC water splitting. Chemosphere **321**, 138007 (2023)
13. G. Mineo, E. Bruno, S. Mirabella, Advances in WO_3-Based Supercapacitors: State-of-the-Art Research and Future Perspectives. Nanomaterials **13**, 1418 (2003)
14. A.V. Salkar, S.V. Bhosale, P.P. Morajkar, Nanostructured WO_{3-x} based advanced supercapacitors for sustainable energy applications, in *Advances in Metal Oxides and Their Composites for Emerging Applications*. (Elsevier, Amsterdam, 2022), pp.213–238
15. F. Zhan, Y. Liu, K. Wang, X. Yang, M. Liu, X. Qiu, J. Li, W. Li, Oxygen-deficient nanofiber WO_{3-x}/WO_3 homojunction photoanodes synthesized via a novel metal self-reducing method. ACS Appl. Mater. Interfaces **11**, 39951–39960 (2019)
16. D. Mandal, P. Routh, A.K. Nandi, A New facile synthesis of tungsten oxide from tungsten disulfide: structure dependent supercapacitor and negative differential resistance properties. Small **1**, 1702881 (2017)
17. Z. Yin, Y. Bu, J. Ren, S. Chen, D. Zhao, Y. Zou, S. Shen, D. Yang, Triggering superior sodium ion adsorption on (2 0 0) facet of mesoporous WO3 nanosheet arrays for enhanced supercapacitance. Chem. Eng. J. **345**, 165–173 (2018)
18. G. Yang, X. Xia Liu, Electrochemical fabrication of interconnected tungsten bronze nanosheets for high performance supercapacitor. J. Power Sources **383**, 17–23 (2018)
19. V.C. Lokhande, T. Hussain, A.R. Shelke, A.C. Lokhande, Taeksoo Ji, Substitutional doping of WO3 for Ca-ion based supercapacitor. Chem. Eng. J. **424**, 130557 (2021)
20. P. Velusamy, S. Liu, R. Xing, M. Sathiya, A. Ahmad, M.D. Albaqami, R.G. Alotabi, E. Elamurugu, M.S. Pandian, P. Ramasamy, Enhanced photo-electrocatalytic performance of the nano heterostructures based on Pr^{3+} modified g-C_3N_4 and BiOI. Int. J. Hydrogen Energy **47**, 32903–32920 (2022)
21. M. Aravind, M. Amalanathan, S. Aslam, A.E. Noor, D. Jini, S. Majeed, P. Velusamy, A.A. Alothman, R.A. Alshgari, M.S. Mushab, M. Sillanpaa, Hydrothermally synthesized Ag-TiO2 nanofibers (NFs) for photocatalytic dye degradation and antibacterial activity. Chemosphere **321**, 138077 (2023)
22. S.P. Gupta, M.A. More, D.J. Late, P.S. Walke, High-rate quasi-solid-state hybrid supercapacitor of hierarchical flowers of hydrated tungsten oxide NSs. Electrochim. Acta **366**, 137389 (2021)
23. M.S. Tamboli, D.P. Dubal, S.S. Patil, A.F. Shaikh, V.G. Deonikar, M.V. Kulkarni, N.N. Maldar, A.M. Asiri, P. Gomez-Romero, B.B. Kale, D.R. Patil, Mimics of microstructures of Ni substituted $Mn_{1-x}Ni_xCo_2O_4$ for high energy density asymmetric capacitors. Chem. Eng. J. **307**, 300–310 (2017)
24. C. Huang, Q. Zhu, W. Zhang, P. Qi, Q. Xiao, Y. Ying, Facile preparation of W5O14 nanosheet arrays with large crystal channels as high-performance negative electrode for supercapacitor Author links open overlay panel. Electrochim. Acta **330**, 135209 (2020)
25. B. Moshofsky, T. Mokari, Length and diameter control of ultrathin nanowires of substoichiometric tungsten oxide with insights into the growth mechanism. Chem. Mater. **25**(8), 1384–1391 (2013)

26. P.J. Boruah, R.R. Khanikar, H. Bailung, Synthesis and characterization of oxygen vacancy induced narrow bandgap tungsten oxide (WO_{3-x}) nanoparticles by plasma discharge in liquid and its photocatalytic activity. Plasma Chem. Plasma Process **40**, 1019–1036 (2020)
27. P. Ivanoff Reyes, C.J. Ku, Z. Duan, Y. Xu, E. Garfunkel, Y. Lu, Reduction of persistent photoconductivity in ZnO thin film transistor-based UV photodetector. Appl. Phys. Lett. **101**(3), 031118 (2012)
28. B. Moshofsky, T. Mokari, Length and diameter control of ultrathin nanowires of substoichiometric tungsten oxide with insights into the growth mechanism. Chem. Mater. **25**, 1384–1391 (2013)
29. S.K. Shinde, D.P. Dubal, G.S., Ghodake, D.Y. Kim, V.J. Fulari, Nanoflower-like CuO/$Cu(OH)_2$ hybrid thin films: Synthesis and electrochemical supercapacitive properties. J. Electroanal. Chem. **732**, 80–85 (2014)
30. S.K. Shinde, M.B. Jalaka, G.S. Ghodake, N.C. Maile, V.S. Kumbhar, D.S. Lee, V.J. Fulari, D.-Y. Kim, Chemically synthesized nanoflakes-like NiCo2S4 electrodes for high-performance supercapacitor application. Appl. Surf. Sci. **466**, 822–829 (2019)
31. K. Sun, F. Hua, S. Cui, Y. Zhu, H. Peng, G. Ma, An asymmetric supercapacitor based on controllable WO 3 nanorod bundle and alfalfa-derived porous carbon. RSC Adv. **11**, 37631–37642 (2021)
32. G. Mineo, E. Bruno, S. Mirabella, Advances in WO3-Based Supercapacitors: State-of-the-Art Research and Future Perspectives. Nanomaterials **13**, 1418 (2023)
33. S.K. Shinde, D.P. Dubal, G.S. Ghodake, V.J. Fulari, Hierarchical 3D-flower-like CuO nanostructure on copper foil for supercapacitors. RSC adv. **5**, 4443–4447 (2015)
34. Z. Khan, B. Senthilkumar, S. Lim, R. Shanker, Y. Kim, H. Ko, Redox-additive-enhanced high capacitance supercapacitors based on $Co_2P_2O_7$ Nanosheets. Adv. Mater. Interfaces **4**, 1700059 (2017)
35. H. Pang, Z. Yan, Y. Ma, G. Li, J. Chen, J. Zhang, W. Du, S. Li, Cobalt pyrophosphate nano/microstructures as promising electrode materials of supercapacitor. J. Solid State Electrochem. **17**, 1383–1391 (2013)
36. R.D. Kumar, Y.A.S. Karuppuchamy, Facile Synthesis of Co—WO3/ functionalized carbon nanotube nanocomposites for supercapacitor applications. J. Mater. Sci. Mater. Electron. **28**, 5425–5434 (2017)
37. J. Jia, X. Liu, R. Mi, N. Liu, Z. Xiong, L. Yuan, C. Wang, G. Sheng, L. Cao, X. Zhou et al., Self-Assembled Pancake-like Hexagonal Tungsten Oxide with Ordered Mesopores for Supercapacitors. J. Mater. Chem. A **6**, 15330–15339 (2018)